18TH WORLD CONFERENCE ON EARTHQUAKE ENGINEERING
WCEE2024
MILAN

MILAN, ITALY
30TH JUNE - 5TH JULY 2024

www.wcee2024.it

# VARIATIONS IN PERFORMANCE IN EXTREME EVENTS WITH SELECTION OF ISOLATION TYPE

Ya-Heng Yang[1], Tracy Becker[2], Takayuki Sone[3] & Takahiro Kinoshita[4]

[1] Ph.D. Student, Department of Civil and Environmental Engineering, University of California, Berkeley, CA 94720. yaheng_yang@berkeley.edu

[2] Associate Professor, Department of Civil and Environmental Engineering, University of California, Berkeley, CA 94720. tcbecker@berkeley.edu

[3] Senior Chief Researcher, Takenaka Research and Development Institute, Chiba, Japan. sone.takayuki@takenaka.co.jp

[4]Associate Chief, Takenaka Corporation, Osaka, Japan. kinoshita.takahiro@takenaka.co.jp

**Abstract**: *While collapse mechanisms for conventional buildings have received considerable attention, they are less well understood for isolated buildings. Regardless of the type of bearing used, it is anticipated that the performance of isolated structures will be comparable under defined ground motion levels. Nevertheless, the probability of building collapse is directly dependent on the bearing failure characteristics, which vary by bearing type. Utilizing various isolation systems while adhering to the same design guidelines may result in varying probabilities of collapse. In this study, the probability of collapse of a three-story buckling-restrained brace frame isolated with double-concave FP bearings or lead rubber bearings is compared. At maximum displacement, various designs are considered, including the use of moat walls versus allowing bearing failure (or impact of the restraining flanges for FP bearings). In the absence of the moat wall, the system-level failure using both bearing types is triggered by exceeding defined displacement capacities. In contrast, with the moat wall, the system-level failure is dominated by either axial component-level failures or excessive yielding of the superstructure. However, when the moat wall restricts ultimate displacement, the disparity in collapse probabilities is small.*

## 1 Introduction

Probability of collapse is used in seismic code specifications with the intent to establish design criteria that align with desired performance objectives for either new or existing buildings under future earthquakes. For example, ASCE 7-22 (ASCE 2022) targets a 10% probability of failure for a typical (non-essential or hazardous) building under maximum considered earthquake (MCER) levels. Assessing the structural collapse performance involves establishing a sufficiently low yet rational probability of collapse, as illustrated by FEMA (2009). In the case of isolated buildings, similar performance ideally should be achieved, regardless of the bearing type selected. While all well-designed and manufactured commonly used isolation bearings provide reliable performance under typical operation, their failure characteristics vary drastically. Thus, it is important to consider bearing design when exploring collapse probability.

Research into the probability of collapse has been recent, and primarily focused on friction pendulum (FP) isolated buildings (Masroor and Mosqueda, 2015; Shao et al., 2017; Bao et al., 2018). Furthermore, previous studies have shown that bearing failure characteristics have a notable impact on assessing the collapse probability of isolated buildings. Bao et al. (2018) explored the influence of rim designs for friction pendulum

(FP) bearings on the performance of isolated buildings, employing a rigid body model to simulate bearing behavior. The model can simulate the response of sliding isolation bearings in extreme scenarios, including impact against restraining rims and subsequent uplift behavior. The study found that changing rim designs can result in a change in the failure mode of the isolated buildings.

Cardone et al. (2019) developed collapse fragility curves for the seismic isolation retrofit of existing buildings, comparing use of FP bearings and high damping rubber bearings (HDR). This assessment was performed by employing the model developed by Kumar et al. (2014). This study found that when using sliding bearings, building collapse is primarily determined by exceeding displacement limits, whereas in the case of HDR bearings, cavitation or buckling dominates the collapse mechanism. However, it should be noted that the study did not consider rim designs of sliding bearings and the impact against moat walls, factors that can significantly influence the results. This study did not explore differences in collapse probability when using the two isolation systems. In a similar fashion, Flora et al. (2020) assesses the collapse probability of existing buildings retrofitted with HDR bearings. This study compared the collapse probability when using either the Kumar HDR model or the Kikuchi HDR model (Kikuchi et al., 2010). The study found that the collapse performance varies depending on the chosen model and the specified failure modes.

There is a lack of studies that compare the collapse probability of building isolated by sliding bearings and rubber bearings. Consequently, the performance differences in code-compliant isolated buildings using these different bearing systems remain unknown. This study addresses this gap by comparing the collapse probabilities of rubber and sliding bearing systems for identical superstructures. The superstructure and isolation systems are designed according to Japanese practice, but the comparison is universal as both isolation systems are designed to the same guidelines with the comparable effective period, effective damping ratio, and displacement capacity. For the sliding bearing system, double concave FP bearings with different rim designs are discussed. For the rubber bearing system, lead rubber bearings (LRB) in combination with flat sliding bearings with rubber pads are used. Several failure characteristics of the bearings are considered, including uplift of sliding bearings and cavitation of rubber bearings. Fragility curves are then developed as a function of earthquake level to compare the probability of collapse for the isolated structure under design level earthquakes given the different isolation layer technology and design.

## 2 Prototype Building and Case Study

### 2.1 Superstructure

A warehouse building is used as the prototype structure. This choice was made due to its potential application for FP bearings in Japan, where FP bearing is increasingly used. The isolated building was designed to exceed the minimum standards of the Japanese Code (Building Standard Law of Japan, BSLJ). To improve the seismic performance of the superstructure, the building has buckling-restrained braces (BRB) around the perimeter with moment restrained gravity framing in the interior, which ensures the effective use of internal space. The arrangement and cross-section of the BRBs are designed in such a way that, under the design-level lateral forces, no undesirable tensile forces are applied to the bearings, in accordance with the requirements of the Japanese code. The basic geometry of the frame is presented in Figure 1. The prototype building is simulated using OpenSees (McKenna et al. 2010). It incorporates concentrated plasticity with rotational springs to represent the nonlinear behavior (Yang et. al., 2023). The BRB is modelled using truss elements with a general uniaxial material with combined kinematic and isotropic hardening (Zsarnoczay 2013).

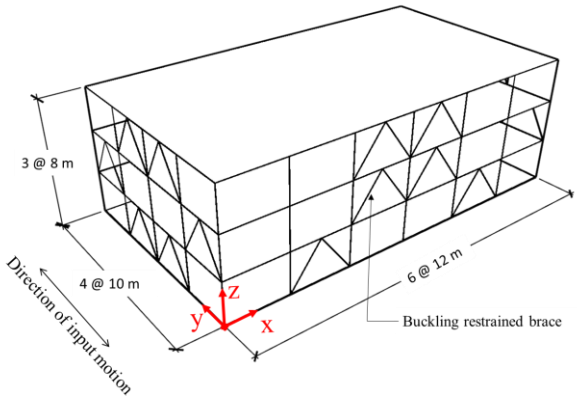


*Figure 1. Prototype building models, BRB frame.*

### 2.2 Isolation systems

Two isolation systems are considered, a sliding bearing system and a rubber bearing system. For the sliding bearing system, double concave FP bearings are used. The bearings vary by the inner slider diameters which is 200 mm, 250 mm, and 350 mm depending on location so that all bearings have similar pressures; displacement diameters are adjusted accordingly so that the displacement limits are the same for all the bearings in the isolation layer. Figure 2(a) shows the layout of the FP bearings where $D_{S1}$ is the diameter of the inner slider. The sliding radius of the bearings $R$ is 8.95 m, resulting in a post-yield period $T_1$ of 6.0 seconds, and the coefficient of friction $\mu$ is 0.047. The double concave FP bearing is modelled using the singleFPBearing element in OpenSees as the radii and friction coefficients of the top and bottom slider are selected to be identical. The Coulomb model (constant coefficient of friction) is used as the importance of velocity and pressure dependencies are relatively low under dynamic ground motion loading (Kumar et al. 2015). The built-in vertical force-deformation relationship of the singleFPBearing element is assumed to be no tensile forces; however, when the bearing uplifts, a small amount of vertical force remains to maintain stability in the numerical analysis. Thus, true uplift behavior is not explicitly modelled.

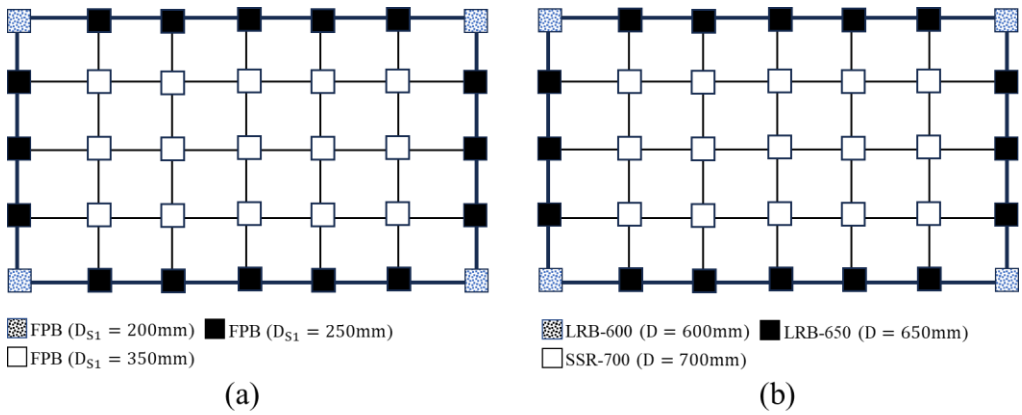


*Figure 2. Layout of isolation layers with: (a) sliding bearings; (b) rubber bearings.*

Sliding bearings with two different rim designs are considered: (1) with a restraining rim and (2) with a flat rim, as shown in Figure 3. The bearing with the restraining rim will have pounding under beyond-design ground motions. This pounding may impart large forces to the superstructure, potentially causing yielding in the superstructure and inducing an uplift behavior in the bearings. The bearings with flat rims have slightly larger displacement capacity as the slider can move onto the flat rims becoming unstable when the inner slider falls from the sliding surface. Note that the size of the FP with a flat rim is smaller than that of the FP with a restraining rim such that the displacement capacity of the different systems is comparable. The rim is modelled using the gap material in OpenSees (Yang et. al., 2023).

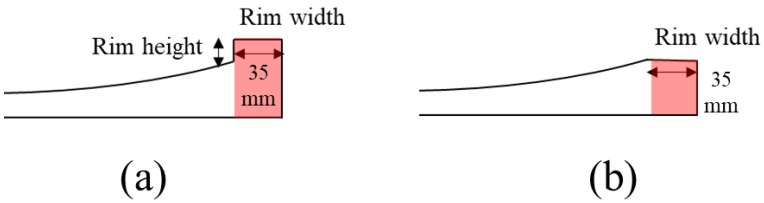


*Figure 3. Different rim designs: (a) restraining rim; (b) flat rim.*

For the rubber bearing system, three types of bearings are used: LRB with outer diameter 600 mm (LRB-600) in the corners, LRB with outer diameter 650 mm (LRB-650) along the periphery, and flat sliding supports with rubber pads (SSR) with outer diameter 700 mm in the interior. The layout of the rubber bearings is shown in Figure 2(b). The sizes of the lead plugs of LRBs are selected so that the hysteretic behavior of the isolation layer would closely match that of the FP bearing system. The response displacement and equivalent period of the isolation layer under the design level are roughly 260 mm and 3.7 s for both arrangements. The LeadRubberX element (Kumar et al. 2014) with modification of the overlapping area method (Yang et. al., 2023) is used for the LRB, and the flatFPBearing element is used for the SSR.

### 2.3 Moat Walls

The Hertzdamp element (Hughes and Mosqueda, 2020; Muthukumar and DesRoches, 2006) is used to simulate pounding against the moat walls. Seven Hertzdamp springs are located on either side of the structure, as shown in Figure 4. The properties of each Hertzdamp spring are defined by the two colliding bodies shown in Figure 4 (Yang et. al., 2023).

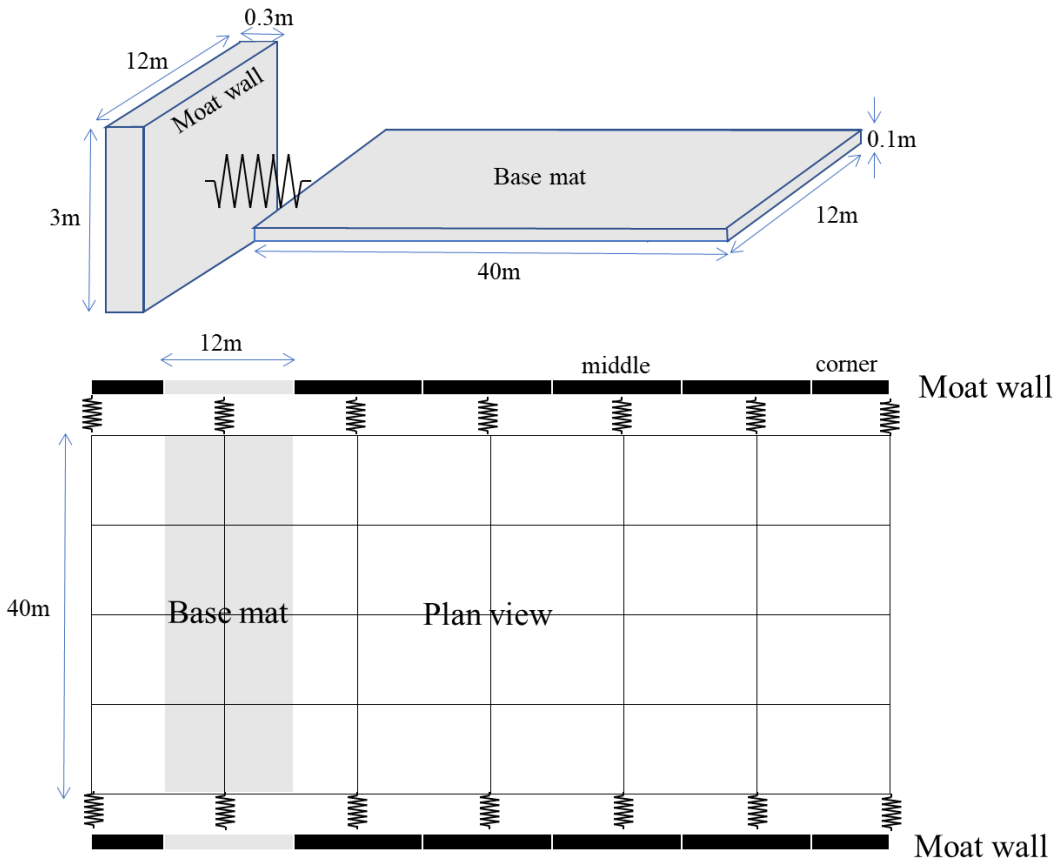


*Figure 4. Definition of the colliding bodies for the Hertzdamp element and the layout of the Hertzdamp element at base level of the isolated building.*

### 2.4 Case Study

Five design cases are investigated, summarized in Table 1.

- Case 1: FP bearings are used without a moat so that the restraining rim of the bearings occurs at 0.60 m.
- Case 2: the FP bearings have flat rims; while the bearing reaches the end of the concave sliding surfaces at a displacement of 0.6 m, bearing failure does not occur until 0.67 m.
- Case 3: the FP bearings and includes moat walls with a gap distance equal to 0.60 m, such that the ultimate displacement of the bearings is not reached.
- Case 4: LRBs are used with a moat wall with a gap distance of 0.60 m (same distance as Case 3).
- Case 5: LRBs are used without moat walls. When a moat wall is included in the design, it is 3 meters high and 0.3 meters thick. In the absence of impact on the moat wall, the base of the building is raised so that the base slab is above ground such that a moat is unnecessary.

The case studies intend to compare the collapse probability of using FP bearings and using LRB under various isolation designs. Case 2 (FP with flat rims) and Case 5 (LRB no moat wall) are compared to evaluate different performance without impact behavior when failure of the bearings is allowed. Case 3 (FP with moat wall) and Case 4 (LRB with moat wall) compares for how moat wall pounding affects the different isolation systems. Case 1 (FP with restraining rims) and Case 4 (LRB with moat wall) are used to compare the response of impacting against a retraining mechanism (either rims or wall) located at the same displacement limit.

*Table 1. The five isolation layer design cases used for comparisons.*

| Case Studies | Descriptions |
|---|---|
| Case 1 | FP no moat wall, restraining rims (impact occurs at 0.60 m) |
| Case 2 | FP no moat wall, flat rims (displacement limit = 0.67 m) |
| Case 3 | FP with moat wall, no rims (impact occurs at 0.60 m) |
| Case 4 | LRB with moat wall (impact occurs at 0.60 m) |
| Case 5 | LRB no moat wall (displacement limit = 0.60 m) |

## 3 Failure Definitions

Failure of the isolated building (system-level failure) is determined based on two categories: excessive yielding of the superstructure leading to instability and failure of the isolation bearing components. Note that the assumption that failure of bearings will result in failure of the entire building may be conservative; however, potential loss of load carrying capacity of the bearings cannot be neglected. In this study, whichever failure condition comes first is defined as the source of the system-level failure. Excess of 2% story drift in the BRB frame is considered as failure, as specified for braced frames in FEMA 356 (FEMA 2000). Regarding to failure of the isolation components, it depends on the isolation system design and is determined by the mechanical characteristics of the bearings. The following paragraphs describe the failure mechanisms for the bearing. The resulting failure definitions for the design case studies are summarized in Table 2 where $\epsilon_t$ is the tensile strain in the rubber bearing, while $\gamma$ is the shear strain in the bearing.

*Table 2. Failure definition for the case studies.*

| Case | Type | Condition | Failure Definition |
|---|---|---|---|
| 1 | FP | Restraining rim | Story drift ratio ≥ 2%, uplift |
| 2 | | Flat rim | $D$ ≥ 670 mm |
| 3 | | Moat wall (600 mm gap) | Story drift ratio ≥ 2%, uplift |
| 4 | LRB | Moat wall (600 mm gap) | Story drift ratio ≥ 2%, $\epsilon_t$ = 20% |
| 5 | | No moat wall | $\gamma_{shear}$ = 300%, $\epsilon_t$ = 20% |

For the FP bearings, failure definitions depend on the rim design (Figure 3). For the bearing with restraining rims, the pounding will impart large forces to superstructure which may result in large uplift of the bearings which can result in their failure. The singleFPBearing element in OpenSees does not explicitly simulate the uplift of the bearings. Instead, the uplift of the FP is modelled with no tension capacity. When the axial force is greater than zero, it is forced to be zero and the tensile stiffness is calculated by multiplying an arbitrary small value to the compressive stiffness. As a result, using an absolute quantity to define uplift, such as a tensile strain of bearings is inappropriate. The failure due to uplift is therefore defined as the element having zero axial force at the same time as when the lateral isolation displacement exceeds its limit of 0.60 m. This definition is only a necessary condition for uplift failure of FP with restraining rims, as the bearing can remain stable even with displacement exceeding 0.6 m due to the flexibility of the restraining rim. Because of this uncertainty, a range of displacement limits, from 0.60 m to 0.61 m, for the failure definition is considered. Note that the failure of the isolated building is determined once one of the bearings has uplifted, which is perhaps conservative.

For the FP bearing with flat rims (Case 2), the slider will fall from the sliding surface when it exceeds the displacement capacity. This displacement is equal to 670 mm (600 mm plus two times the rim width of 35 mm, as shown in Figure 3b). For the FP with moat walls (Case 3), the failure due to uplift is defined as having zero axial force and having a lateral isolation displacement exceeding 0.60025 m, i.e., 0.6 m plus half of the maximum expected indentation, which is also to account for uncertainty in defining failure due to uplift.

For the LRBs, two ultimate states are defined: shear rupture and cavitation. Shear rupture is determined as 300% shear deformation of bearings, which corresponds to 600 mm lateral displacement. Note that under 6 MPa which is close to the average axial load on the bearings, negative stiffness begins to occur at about 245% strain; however, the load-bearing and horizontal resistance capacity are not immediately lost. Therefore, the assumption of the same deformation capacity (600 mm or 300% strain) as the FP bearing in the collapse evaluation is adopted. Cavitation is determined at 20% axial tensile strain in a bearing (Kani et al., 1999), computed as the ratio of axial deformation to the distance between two nodes of the bearing. Buckling is not considered as an ultimate state since the bearing can maintain an effective capacity after buckling due to its post-buckling behavior.

## 4 Collapse Probability

The collapse probabilities of the five case studies are found using the multiple stripe analysis method with the 22 near-fault motions and 22 far-field motions scaled from Level 2. The selection and scaling procedures for the ground motions can be found in Yang et. al. (2023). The fragility curve of the five design cases under near-fault and far-field motions is presented in Figure 5(a) and Figure 5(b), respectively. Only the record-to-record variability directly from the ground motion results is included. Values of 1.0 and 1.5 for the scale factor correspond to Level 2 and Level 3, respectively. The highlighted area shown in Figure 5 represents a range in predicted fragility functions for the case using FP with restraining rims (Case 1), when considering uplift failure as occurring with zero tensile force at displacements ranging from 0.60 m to 0.61 m. The red dashed line for Case 1 represents the fragility function considering uplift failure occurs when the isolation displacement exceeds 0.605 m.

To assess the seismic collapse safety of each case study, the collapse margin ratio (CMR) introduced by FEMA P695 (FEMA 2009) is used. The CMR is defined as the ratio of scale factor relative to Level 3 at which half of the suite of ground motions cause collapse. CMR can be interpreted as the degree by which the scale factor for Level 3 motion must be increased to achieve a 50% collapse of the isolated building. A higher CMR value indicates a better collapse performance of the structure. In Figure 5, CMR is represented by the scale factor corresponding to a 50% collapse probability, divided by 1.5. The CMR values for each case study are presented in Table 3.

Comparing the case using FP with flat rims (Case 2) with the case using LRB without a moat wall (Case 5), FP bearings have a larger CMR regardless of the type of input motions, 1.71 versus 1.48 and 1.70 versus 1.43 for near-fault and far-field, respectively. The FP with flat rims has a slightly higher displacement capacity (670 mm), whereas the shear strain limit of LRBs is 300%, which corresponds to 600 mm of lateral displacement. Further, because of the strength degradation in the LRB, excessive lateral displacement of LRBs may occur at lower intensities than for the FP bearings leading to earlier failure.

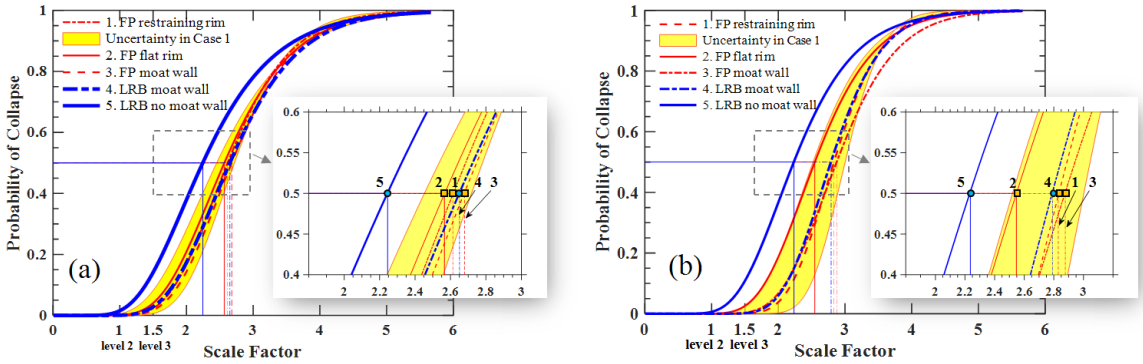


*Figure 5. Fragility curves of the isolated building: (a) near-fault motions; (b) far-field motions.*

When the moat wall is used in the design (Case 3 versus Case 4), the failure mechanisms switch from excessive bearing displacement to bearing axial tensile failure or excessive yielding of the superstructure. Pounding from the moat wall decreases the difference between the fragility curves of the FP system and the LRB systems (Figure 5). The CMR of FP bearings and LRBs becomes closer, 1.79 versus 1.78 and 1.92 versus 1.87 for near-fault and far-field, respectively. Therefore, if impact is incorporated into the ultimate design of the isolated building, the shear behavior of the bearing becomes less significant in determining the collapse performance.

The CMR when using FP with restraining rims (Case 1) is similar to that of using LRB with the moat wall gap of 0.6 m gap (Case 4), 1.74 versus 1.78 and 1.89 versus 1.87 for near-fault and far-field, respectively. This can also be observed in comparison of FP with restraining rims (Case 1) and FP with moat wall (Case 3). Note that the impact force developed with a moat wall is higher than with restraining rims, which results in higher maximum drift ratios; however, a similar CMR is observed based on the assumed failure modes. If the failure due to uplift is not considered in Case 3 as FP bearing failure may be mitigated by the constrain of the moat wall, only excess yielding in the superstructure is considered as collapse for Case 3, and the CMR of Case 3 will be larger (2.02) than that of Case 1 (1.74) under near-fault motions. Thus, collapse probability estimations will differ based on the assumptions of failure modes. Among the five case studies, if impact is incorporated into the ultimate design of the isolated building, lower collapse probabilities are observed; this is more significant for the isolated building subjected to the far-field motions.

*Table 3. Collapse margin ratio of each of the design cases.*

| Case | Type | Condition | Collapse Margin Ratio relative to Level 3 | |
|---|---|---|---|---|
| | | | near-fault | far-field |
| 1 | FPB | Restraining rim | 1.74 (2.08)* | 1.89 (2.18) |
| 2 | | Flat rim | 1.71 (1.71) | 1.70 (1.70) |
| 3 | | Moat wall (0.60 m gap) | 1.79 (2.02) | 1.92 (2.17) |
| 4 | LRB | Moat wall (0.60 m gap) | 1.77 (1.98) | 1.87 (2.08) |
| 5 | | No moat wall | 1.50 (1.50) | 1.48 (1.48) |

*Values in the parenthesis represent the case without axially component-level failure

The relation between component-level bearing failures and system-level failures remains an unresolved issue. In this context, it is assumed that the failure of a single bearing will lead to the failure of the entire structure. This is a conservative decision. To explore the effects of excluding cavitation or uplift of individual bearings as failure mechanisms, Table 3 also shows CMR value if only excessive yielding of the superstructure and bearing displacement is included as the failure conditions (value in the parenthesis). The value is much higher than that including cavitation or uplift of individual bearings and we believe that this might underestimate the collapse probabilities of the isolated structure.

## 5 Conclusion

This paper compares the collapse probabilities of a Japanese designed BRB building isolated with either FP bearing or LRB. Various factors that influence the structural response are included: nonlinear response of the superstructure, bearing failure characteristics, impact with moat walls, and different rim designs for the FP bearings. The comparisons indicated that using different isolation systems while following the same design guidelines results in different collapse probabilities. According to the record-to-record CMR values, FP bearings with flat rims outperform LRBs in terms of collapse probabilities, due to the increased displacement capacity and removal of the pounding from the moat wall. Using FP bearings with restraining rims displays similar performance to using LRBs with comparable displacement capacity before impact. However, when considering the impact against the moat wall for the building isolated with FP bearings, the disparity in fragility curves between the FP bearing system and the LRB system becomes less pronounced.

The definition of system-level failure significantly influences the calculated collapse probability. In the designs under consideration, component-level failures, such as cavitation of LRBs and uplift of FP bearings, typically occur before the superstructure experiences excessive yielding following an impact. Consequently, considering only drift ratio and horizontal isolator displacement as failure mechanisms leads to an overestimation of structural behavior and CMR. However, in comparing the buildings with FP bearing and LRB, even if only the drift ratio and the horizontal isolator displacement are considered, the collapse probability of when using FP bearing is generally slightly lower than with LRB because of the softening behavior of LRB. These results are, of course, dependent on the specific bearing design and the assumptions of failure modes. For example, floor acceleration may be considered a failure mode for the superstructure if non-structural components are of greater concern. Nevertheless, these results highlight that collapse probability of an isolated building will vary even when employing the same design principals, equations with equivalent lateral design procedures based on the bearing type selected.

## 6 Acknowledge

The authors would like to thank Dr Masashi Yamamoto of the Takenaka Research and Development Institute for valuable comments on the study. We also would like to thank Mr. Yuta Kurokawa for assisting the structural design of seismically isolated building. Funding for this study was provided by Takenaka Corporation, which is gratefully acknowledged here.

## 7 References

American Society of Civil Engineers (2022). *Minimum design loads and associated criteria for buildings and other structures*. American Society of Civil Engineers.

Bao, Y., Becker, T.C., Sone, T. and Hamaguchi, H. (2018). To limit forces or displacements: collapse study of steel frames isolated by sliding bearings with and without restraining rims. *Soil Dynamics and Earthquake Engineering*, *112*, pp.203-214.

Cardone, D., Perrone, G., and Piesco, V. (2019). Developing collapse fragility curves for base- isolated buildings. *Earthquake Engineering & Structural Dynamics*, 48(1), 78–102.

FEMA (2000). *Prestandard and Commentary for the Seismic Rehabilitation of Buildings*. Rep. No. FEMA-356, Washington, D.C.

FEMA (2009). *Quantification of building seismic performance factors*. Rep. No. FEMA-P695, Washington, D.C.

Flora, A., Perrone, G., and Cardone, D. (2020). Evaluating collapse fragility curves for existing buildings retrofitted using seismic isolation. *Applied Sciences*, 10(8), 2844.

Hughes, P. J. and Mosqueda, G. (2020). Evaluation of uniaxial contact models for moat wall pounding simulations. *Earthquake Engineering & Structural Dynamics*, 49(12), 1197–1215.

Kani, N., Iwabe, N., Takayama, M., Morita, K., and Wada, A. (1999). Experimental study on the tension capacity in the displaced position of elastomeric isolators part 3 tests of effect of tensile loading. *Summaries of Technical Papers of Annual Meeting, Architectural Institute of Japan*, 563–564. (In Japanese)

Kikuchi, M., Nakamura, T., and Aiken, I. D. (2010). Three-dimensional analysis for square seismic isolation bearings under large shear deformations and high axial loads. *Earthquake engineering & structural dynamics*, 39(13), 1513–1531.

Kitayama, S. and Constantinou, M. C. (2018). Collapse performance of seismically isolated buildings designed by the procedures of ASCE/SEI 7. *Engineering Structures*, 164, 243–258.

Kumar, M., Whittaker, A. S., and Constantinou, M. C. (2014). An advanced numerical model of elastomeric seismic isolation bearings. *Earthquake engineering & structural dynamics*, 43(13), 1955–1974.

Kumar, M., Whittaker, A. S., and Constantinou, M. C. (2015). Characterizing friction in sliding isolation bearings. *Earthquake engineering & structural dynamics*, 44(9), 1409-1425.

Masroor, A. and Mosqueda, G. (2015). Assessing the collapse probability of base-isolated buildings considering pounding to moat walls using the FEMA P695 methodology. *Earthquake Spectra*, 31(4), 2069–2086.

McKenna, F., Scott, M. H., and Fenves, G. L. (2010). Nonlinear finite-element analysis software architecture using object composition. *Journal of Computing in Civil Engineering*, 24(1), 95– 107.

Ministry of Land, Infrastructure, Transport and Tourism. *The Building Standard Law of Japan*. Japan.

Muthukumar, S. and DesRoches, R. (2006). A hertz contact model with non-linear damping for pounding simulation. *Earthquake engineering & structural dynamics*, 35(7), 811–828.

Shao, B., Mahin, S., and Zayas, V. (2017). Member capacity factors for seismic isolators as required to limit isolated structure collapse risks to within ASCE 7 stipulated structure collapse risk limits. *Report No. UCB/SEMM-2017/02*, Structural Engineering, Mechanics and Materials, Department of Civil and Environmental Engineering University of California, Berkeley, Berkeley, Calif.

Yang, Y. H., Becker, T. C., Sone, T., & Kinoshita, T. (2023). Sliding versus Rubber Bearings: Exploring the Difference in Collapse Probability. *Journal of Structural Engineering*, *149*(7), 04023086.

Zsarnóczay, Á. (2013). Experimental and numerical analysis of buckling restrained braced frames for Eurocode conform design procedure evaluation. Ph.D. thesis, BME Department of Structural Engineering, Budapest.